




Shared LO-based self-coherent 16QAM transmission with PTBC for cost-sensitive metro networks

Jongwan Kim ^a , Sang-Rok Moon ^a, Sun Hyok Chang ^a, Hun-Sik Kang ^a, Sunghyun Bae ^b ,* 

^a Network Research Division, Electronics and Telecommunications Research Institute (ETRI), 218 Gajeong-ro, Yuseong-gu, 34129, Daejeon, Republic of Korea

^b Department of Quantum Information Science and Engineering, Sejong University, 209 Neungdong-ro, Gwangjin-gu, 05006, Seoul, Republic of Korea

ARTICLE INFO

Keywords:

Polarization-time block code
Self-coherent
Shared local oscillator

ABSTRACT

We propose a cost-effective architecture for >100-Gb/s metro networks with an 80-km reach, utilizing Alamouti polarization-time block code (PTBC), a self-coherent scheme, and a shared-local oscillator (LO) configuration. The combination of PTBC and the self-coherent scheme enables the use of a single-polarization coherent receiver without carrier recovery algorithms. While conventional self-coherent schemes typically require two fiber strands to transmit a single signal, the proposed shared-LO configuration allows a single LO to serve multiple signal channels, thereby improving fiber utilization efficiency. We experimentally demonstrate the transmission of 120- and 240-Gb/s PTBC 16-QAM signals over 80 km of single-mode fiber. A power budget analysis, based on our experimental results, shows that a single LO can support up to 15 and 7 signal channels for the 120- and 240-Gb/s systems, respectively, assuming a 16-dBm laser output power.

1. Introduction

The rapid proliferation of Internet traffic driven by artificial intelligence (AI), video streaming services, and mobile communications necessitates the deployment of high-speed metropolitan networks over distances ranging from 40 to 80 km [1–4]. In particular, the explosive growth of AI-driven services has led to massive data center expansion, creating a strong demand for inter-data center interconnects over reaches of up to 80 km [1,5]. However, the effects of chromatic dispersion (CD) cannot be neglected when transmitting signals at data rates exceeding 100 Gb/s over 80 km using intensity modulation and direct detection systems [5–7]. For example, when transmitting four-level pulse amplitude modulation (PAM4) signals in the O band, which exhibits low CD, transmitting 100-Gb/s signals over 80 km may require > 50-tap second-order nonlinear equalizers [2], potentially requiring even third-order nonlinear equalizers for 200-Gb/s signals [4]. Although CD can be effectively compensated when using coherent systems, enabling the transmission across the full C-band spectrum, their deployment in metro networks is limited by the high cost, complexity, and power consumption [8,9]. As a result, there is growing interest in coherent-lite approaches that preserve the key advantages of coherent detection, especially digital CD compensation, while reducing cost and complexity.

One promising coherent-lite technique is Alamouti polarization-time block coding (PTBC), which enables a single-polarization coherent receiver by employing transmitter-side polarization diversity [8,10].

This configuration alleviates the challenges associated with the monolithic integration of a polarization-diverse coherent receiver [8], and reduces the required number of analog-to-digital converters [11,12]. Although PTBC necessitates a dual-polarization transmitter, it offers more stable operation than dynamic polarization control (DPC)-based systems under rapid polarization fluctuations (down to microsecond timescales) through digital signal processing (DSP)-based channel adaptation [13,14]. The spectral efficiency penalty from not exploiting polarization-division multiplexing can be compensated by employing advanced modulation formats such as 16-ary quadrature amplitude modulation (16QAM) [15,16]. However, the practical implementation of a conventional PTBC decoder can be challenging, since it requires the simultaneous estimation of slowly-varying channel effects, including polarization rotation, and fast-varying carrier phase noise [17].

Another viable coherent-lite approach is the self-coherent transmission system, in which the local oscillator (LO) is transmitted along with the modulated signal from the transmitter [5,9,18]. This scheme eliminates the need for a separate LO at the receiver, significantly relaxing requirements on laser linewidth and wavelength alignment [5, 18]. Moreover, self-coherent architectures can substantially reduce DSP complexity by removing the carrier frequency offset (CFO) recovery and carrier phase estimation (CPE) blocks [18]. However, conventional self-coherent systems typically require duplex fiber links, where the signal and LO are transmitted over separate fibers, resulting in only

* Corresponding author.

E-mail address: sungbae@sejong.ac.kr (S. Bae).

50% fiber utilization efficiency [18]. In addition, they require polarization alignment between the signal and LO [18], which may pose considerable implementation challenges under dynamic polarization conditions.

In this work, we propose a high-speed transmission system for metro networks by combining PTBC with a self-coherent scheme. This integration enables a simplified single-polarization receiver without carrier recovery blocks (CFO/CPE). To improve fiber utilization efficiency, we introduce a shared-LO configuration where a single laser output is split at the receiver to support multiple signal lanes, making it suitable for multi-strand fibers such as ribbon fibers [19], or potentially multi-core fibers [20]. Notably, the proposed shared-LO architecture is also compatible with a single-polarization receiver employing DPC. We experimentally validate this architecture by transmitting 120- and 240-Gb/s PTBC-16QAM signals over 80-km fiber and present a comprehensive power budget analysis to quantify system scalability. This study extends our previous work presented at the conference [21], where the integration of PTBC and self-coherent schemes was initially proposed for a passive optical network.

The remainder of this paper is organized as follows. Section 2 describes the architecture of the proposed optical transmission system. Section 3 presents experimental results demonstrating 120- and 240-Gb/s PTBC-16QAM transmissions. Section 4 provides a power budget analysis without signal amplification. Finally, Section 5 summarizes the paper.

2. Proposed metro network architecture

2.1. System architecture

Fig. 1(a) shows the configuration of the proposed system which integrates PTBC, a self-coherent scheme, and a shared-LO architecture. The laser output is split into N branches, with one branch used as an LO, and the remaining $(N - 1)$ branches converted into PTBC-16QAM signals, as illustrated in Fig. 1(b). Specifically, two complex 16QAM symbols $[s_1, s_2]$ are encoded into two PTBC codewords as $[s_1, -s_2^*]$ and $[s_2, s_1^*]$ over two symbol periods. In the dual-polarization IQ modulator (DP-IQM), the light is first split into two orthogonal polarizations by a polarization beam splitter (PBS); each polarization is then modulated with one of the codewords before being recombined by a polarization beam combiner (PBC). The LO and the $(N - 1)$ PTBC signals are transmitted over multi-strand fibers. At the receiver, the transmitted LO is amplified by an optical amplifier (OA) to provide high output power (e.g. up to 20 dBm) and then split into $(N - 1)$ branches. Finally, $(N - 1)$ coherent receivers are used to reconstruct the original $(N - 1)$ data streams. As illustrated in Fig. 1(c), each coherent receiver mixes its corresponding signal with a split LO using an optical hybrid, and two balanced photodiodes (BPDs) are used to detect both the in-phase (I) and quadrature (Q) components.

Crucially, the LO should be amplified on the receiver side to avoid stimulated Brillouin scattering (SBS). Amplifying the LO at the transmitter would trigger SBS, which in turn significantly increases the signal's propagation loss. In addition, the proposed architecture is scalable for wavelength-division multiplexing systems. In such implementations, it is advantageous to demultiplex the amplified LO into individual wavelength components at the receiver side, prior to optical splitting. The additional loss introduced by the demultiplexer must be taken into account when designing the system, as it directly affects the required LO amplification level.

2.2. PTBC decoder in self-coherent system

In an ideal channel without inter-symbol interference (ISI) from effects like CD, the input-output relationship for two consecutive symbols can be expressed as

$$\begin{bmatrix} r_1 \\ r_2^* \end{bmatrix} = \begin{bmatrix} h_{xx} & h_{xy} \\ h_{xy}^* & -h_{xx}^* \end{bmatrix} \begin{bmatrix} s_1 \\ s_2 \end{bmatrix}, \quad (1)$$

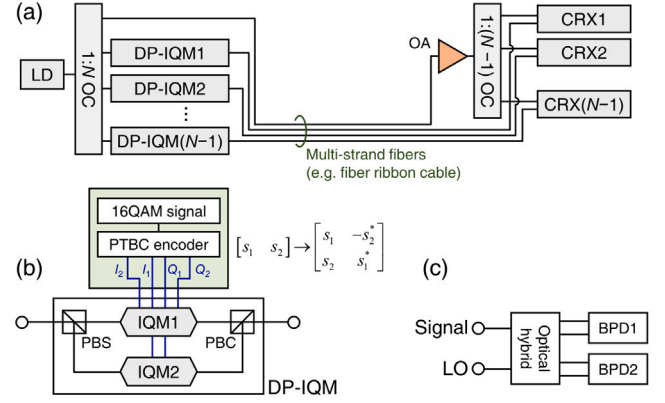


Fig. 1. (a) Configuration of the proposed transmission system utilizing PTBC, a self-coherent scheme, and a shared-LO architecture. (b) Block diagram of the DP-IQM for generating PTBC-16QAM signals. (c) Block diagram of the single-polarization coherent receiver. (BPD: balanced photodetector, CRX: coherent receiver, DP-IQM: dual-polarization IQ modulator, LD: laser diode, LO: local oscillator, OA: optical amplifier, OC: optical coupler, PBC: polarization-beam combiner, PBS: polarization-beam splitter, PTBC: polarization-time block code).

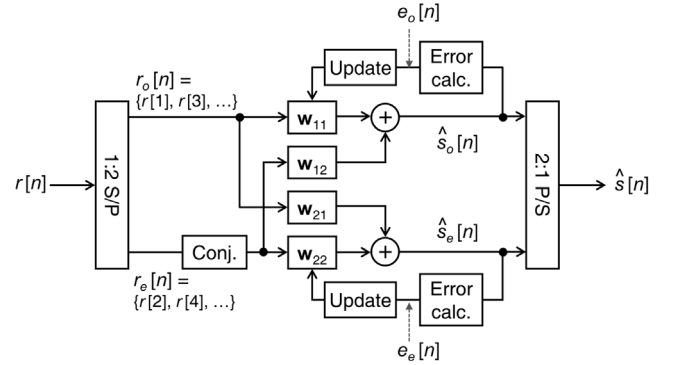


Fig. 2. Schematic of the proposed PTBC decoder. (Conj.: complex conjugation, P/S: parallel to serial, S/P: serial to parallel).

where h_{xx} and h_{xy} represent the elements of the channel's Jones matrix $H = [h_{xx}, h_{xy}; h_{yx}, h_{yy}]$, s_k denotes the k th transmitted symbol, and r_k denotes the corresponding received symbol. Notably, this expression does not require taps for CPE, a direct benefit of the self-coherent scheme. Since the matrix $[h_{xx}, h_{xy}; h_{xy}^*, -h_{xx}^*]$ is unitary, the transmitted symbols can be estimated as

$$\begin{bmatrix} \hat{s}_1 \\ \hat{s}_2 \end{bmatrix} = \begin{bmatrix} h_{xx}^* & h_{xy} \\ h_{xy}^* & -h_{xx} \end{bmatrix} \begin{bmatrix} r_1 \\ r_2 \end{bmatrix}, \quad (2)$$

where \hat{s}_k denotes the k th estimated symbol at the receiver. This indicates that the original transmitted symbols can be recovered by a simple linear transformation, without CFO and CPE blocks.

Fig. 2 shows the schematic of the PTBC decoder. The received signal $r[n]$ is separated into two interleaved sequences: $r_o[n]$, consisting of the odd-indexed samples (i.e., $\{r[1], r[3], \dots\}$), and $r_e[n]$, consisting of the even-indexed samples (i.e., $\{r[2], r[4], \dots\}$). These two sequences are then processed by a 2×2 multiple-input multiple-output (MIMO) equalizer, expressed as

$$\hat{s}_o[k] = w_{11} * r_o[k] + w_{12} * r_e^*[k], \quad (3a)$$

$$\hat{s}_e[k] = w_{21} * r_o[k] + w_{22} * r_e^*[k], \quad (3b)$$

where $r_o[k]$ and $r_e[k]$ denote sampled vectors centered at index k , defined as $\{r_o[k - N], \dots, r_o[k + N]\}$ and $\{r_e[k - N], \dots, r_e[k + N]\}$,

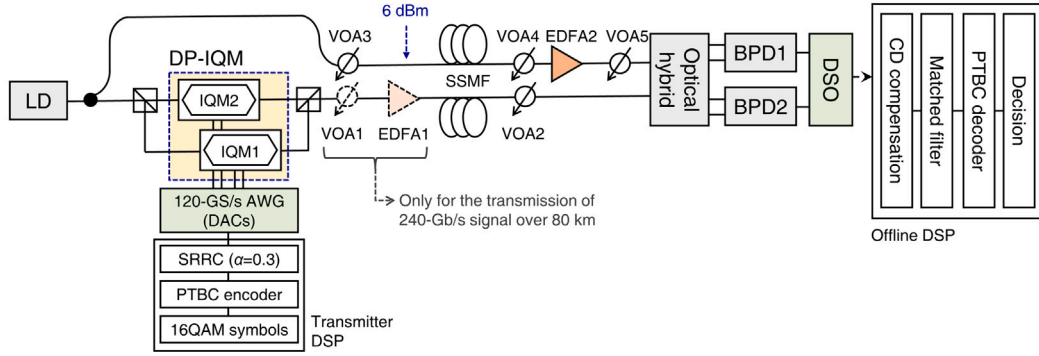


Fig. 3. Experimental setup for 120- and 240-Gb/s PTBC-16QAM signal transmission. (AWG: arbitrary waveform generator, CD: chromatic dispersion, DAC: digital-to-analog converter, DSO: digital sampling oscilloscope, EDFA: erbium-doped fiber amplifier, SSMF: standard single-mode fiber, SRRC: square root-raised cosine filter, VOA: variable optical attenuator).

respectively, and N is the number of pre- and post-cursor taps. Each w_{mn} (for $m, n \in \{1, 2\}$) represents the impulse response of a finite impulse response (FIR) filter that forms the 2×2 MIMO equalizer and compensates for polarization rotation [22]. No separate tap is needed for CPE, owing to the use of a self-coherent scheme.

Then, the errors are calculated as

$$e_{o/e}[k] = d_{o/e}[k] - \hat{s}_{o/e}[k], \quad (4)$$

where $d_{o/e}[k]$ denotes the k th training symbol (in training mode) or the decision-directed (DD) symbol corresponding to $\hat{s}_{o/e}[k]$. The filter coefficients are then updated using the least mean square algorithm as follows:

$$w_{11}[k+1] = w_{11}[k] + \mu e_o[k] r_o^*[k], \quad (5a)$$

$$w_{12}[k+1] = w_{12}[k] + \mu e_o[k] r_e^*[k], \quad (5b)$$

$$w_{21}[k+1] = w_{21}[k] + \mu e_e[k] r_o^*[k], \quad (5c)$$

$$w_{22}[k+1] = w_{22}[k] + \mu e_e[k] r_e^*[k], \quad (5d)$$

where μ is the step size, and $w_{mn}[k]$ denotes the FIR coefficients applied to the k th symbol vectors. The 2×2 MIMO equalizer compensates for residual ISI and polarization-dependent impairments such as polarization-mode dispersion. Unlike conventional PTBC decoders, the PTBC decoder shown in Fig. 2 remains robust to faster laser phase noise fluctuations without requiring explicit tracking.

3. Experiments on 120- and 240-Gb/s PTBC-16QAM transmission

Fig. 3 shows the experimental setup for transmitting 120- and 240-Gb/s PTBC-16QAM signals. Although the proposed architecture in Fig. 1(a) involves splitting the laser output into N branches, this experiment was conducted by splitting the laser output into only two tributaries to evaluate the BER performance of a single channel. In experiments requiring signal amplification with an erbium-doped fiber amplifier (EDFA1) (for transmitting the 240-Gb/s PTBC signal over 80 km), a variable optical attenuator (VOA1) was used to emulate the optical signal-to-noise ratio (OSNR) degradation from increased branching (i.e., large N). For unamplified transmissions, the impact of signal power reduction from an N -way split was emulated by adjusting VOA2 at the receiver. Separately, the corresponding LO power reduction was emulated by VOA3 at the transmitter.

The output of a laser diode (LD) (14.0-dBm power, 25-kHz linewidth) was split into two branches; one with 10.4 dBm was used as the transmitted LO, and the other with 10.0 dBm was used to generate the PTBC-16QAM signal via a DP-IQM. The DP-IQM was driven by four electrical signals generated from a 120-GS/s arbitrary waveform generator (AWG); these signals were created by Alamouti-encoded 16QAM signals, followed by pulse-shaping with a square root-raised

cosine (SRRC) filter (roll-off factor (α) = 0.3). In the experiments demonstrating the transmission of a 240-Gb/s signal over an 80-km fiber, the launched optical power was controlled using VOA1 and EDFA1. The signal and transmitted LO were delivered through two separate standard single-mode fiber (SSMF) spools. For the 40- and 80-km transmission experiments, fiber spool pairs with lengths of (40.01 km, 40.42 km) and (80.43 km, 81.72 km) were employed for the signal and LO paths, respectively. The phase mismatch caused by the path-length difference was not compensated. The received signal and LO power were controlled by VOA2 and VOA4, respectively, to assess the power budget. Subsequently, the LO was amplified by EDFA2 and further adjusted using VOA5 to evaluate the impact of the receiver-side LO splitting, which can reduce the shot-noise dominance of the coherent receiver. After the signal was mixed with the transmitted LO, it was detected by two BPDs and sampled by a digital sampling oscilloscope (DSO) (sampling rate = 256 GSample/s, bandwidth = 40 GHz). In offline DSP, the sampling timing was estimated using a matched filter, CD was compensated, and the PTBC signals were decoded.

To ensure shot-noise-dominant detection, a high LO power at the receiver is desirable. However, our experimental results revealed that when the LO launch power exceeded 6 dBm, high received LO power could not be achieved after 40- and 80-km SSMF transmission due to SBS. As shown in Fig. 4(a), when the output power of the 1549.7-nm laser was increased from 0 dBm to 12 dBm without fiber transmission, the optical spectrum retained its shape, with only the power increasing proportionally. In contrast, once the LO was transmitted through the 40- and 80-km fiber, new frequency components due to SBS emerged for launch powers exceeding 6 dBm, as shown in Figs. 4(b) and 4(c), respectively. Further measurements of the received optical power after 40- and 80-km SSMF showed that increasing the launch power beyond 8 dBm no longer led to an increase in received power, indicating saturation caused by SBS (see Figs. 4(d) and 4(e)). The insertion loss remained nearly constant for launch powers below 6 dBm. Based on these observations, the launch power was set to 6 dBm to avoid nonlinear effects. However, when the 6-dBm LO was transmitted over tens of kilometers of fiber and subsequently split for multi-lane detection, shot-noise dominance can no longer be maintained. Therefore, an optical amplifier (EDFA2) was required at the receiver to boost the LO power.

We evaluated the BER performance for the 120-Gb/s PTBC-16QAM signals using the available components, as illustrated in Fig. 5(a). The tap lengths of the PTBC decoder were set to 11, 17, and 23 for the back-to-back, 40-km, and 80-km transmission cases, respectively. In the back-to-back case, a directly split 10.4-dBm laser output was used as the LO without EDFA2, achieving a receiver sensitivity (at a BER of 10^{-2}) of -32.3 dBm. For the 40- and 80-km transmission cases, the LO launch power was set to 6-dBm and subsequently amplified to 10.4-dBm using the EDFA2 at the receiver side. After 40- and 80-km

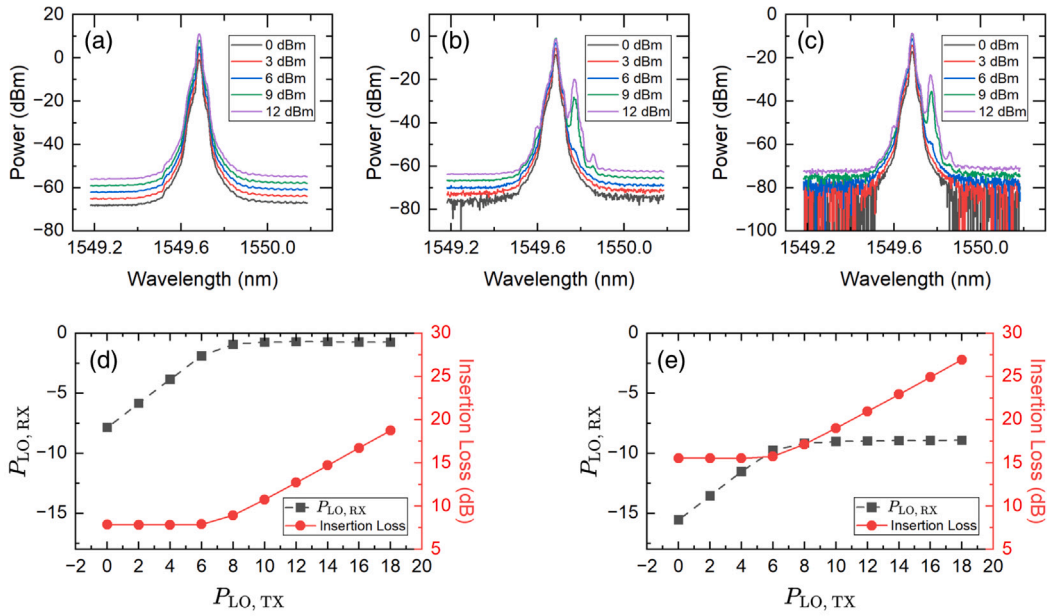


Fig. 4. (a) Optical spectra of the transmitted LO measured at various fiber launch powers. Optical spectra of the received LO after (b) 40-km and (c) 80-km SSMF transmission, respectively, at various fiber launch powers. Received LO power and corresponding insertion loss after (d) 40-km and (e) 80-km SSMF, respectively, as a function of the transmitted LO power.

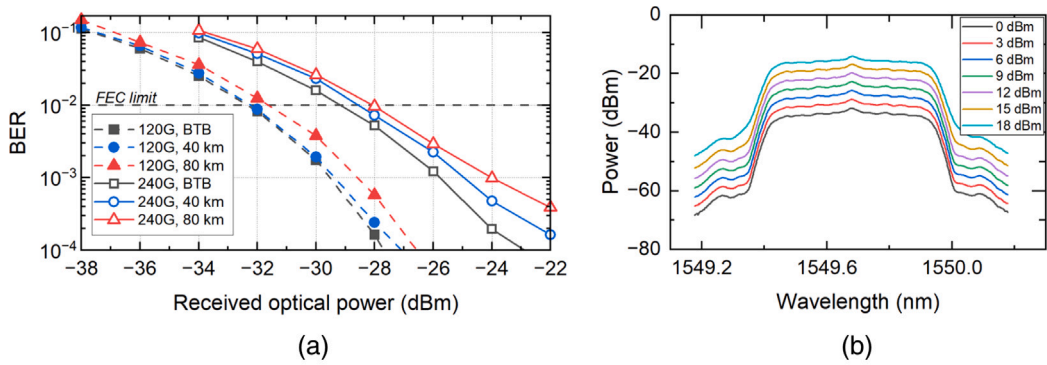


Fig. 5. (a) BER performance of the 120- and 240-Gb/s PTBC-16QAM signals over back-to-back, 40-, and 80-km links using a directly split 10.4-dBm LO. (b) Optical spectra of 240-Gb/s signals after 80-km SSMF transmission at different fiber launch powers. (FEC: forward error correction).

transmission, the receiver sensitivity degraded by 0.3 dB and 0.6 dB, respectively, primarily due to the LO OSNR degradation. Similarly, the BER performance for the 240-Gb/s signals was investigated. The PTBC decoder tap lengths were configured as 19, 25, and 31 for the back-to-back, 40-km, and 80-km transmission cases, respectively. As with the 120-Gb/s back-to-back experiment, the directly split 10.4-dBm LO was used without EDFA2. For the 80-km case, the signal was amplified to 6 dBm at the transmitter using the EDFA1 to evaluate the BER performance down to -22 dBm, as shown in Fig. 5(a) and to compensate for the high insertion loss (up to 15 dB) of the employed DP-IQM (ID Photonics, OMFT class 60), ensuring a sufficient link budget. As shown in Fig. 5(b), the effect of SBS on the 240-Gb/s signal was negligible, and the use of EDFA1 had little effect on the BER performance. The receiver sensitivity penalties after 40- and 80-km transmission were measured to be 0.7 dB and 1.2 dB, respectively, exhibiting a trend similar to that of the 120-Gb/s measurements.

We investigated the impact of the EDFA input LO power on BER performance under back-to-back conditions, as shown in Figs. 6(a) and 6(b). For this test, the EDFA's output LO power was fixed at 10.4 dBm, and the PTBC decoder tap lengths for the 120- and 240-Gb/s signals were set to 11 and 19, respectively. For the 120-Gb/s

signal, the receiver sensitivity at a BER of 10^{-2} was measured to be -31.9 dBm when the EDFA input LO power was -10 dBm. As the input power decreased, the sensitivity gradually degraded due to the reduced LO OSNR of < 43 dB, lower than the transmitter-side OSNR of 63 dB. For the 240-Gb/s signal, a baseline sensitivity penalty of 3.2 dB was observed at a high LO input power of -10 dBm compared to the 120-Gb/s case, primarily due to the doubled data rate. However, as the input LO power was reduced to -22 dBm, an additional penalty arising from the OSNR degradation was superimposed on the data-rate penalty, increasing the total measured penalty to 4.1 dB. As shown by comparing Figs. 6(a) and 6(b), the overall degradation trend as a function of the EDFA input LO power for the 240-Gb/s case was similar to that of the 120-Gb/s case.

Next, we experimentally examined the impact of the amplified LO output power on the BER, with the EDFA input power fixed at -15 dBm, as shown in Figs. 6(c) and 6(d). For the 120-Gb/s signal, the receiver sensitivity remained constant at -31.1 dBm for LO output powers between 9 dBm and 13 dBm, as shown in Fig. 6(c). These results indicated that the BER performance saturated when the EDFA output LO power exceeded 9 dBm, suggesting that shot-noise-dominant reception was achieved above this threshold. Conversely, when the

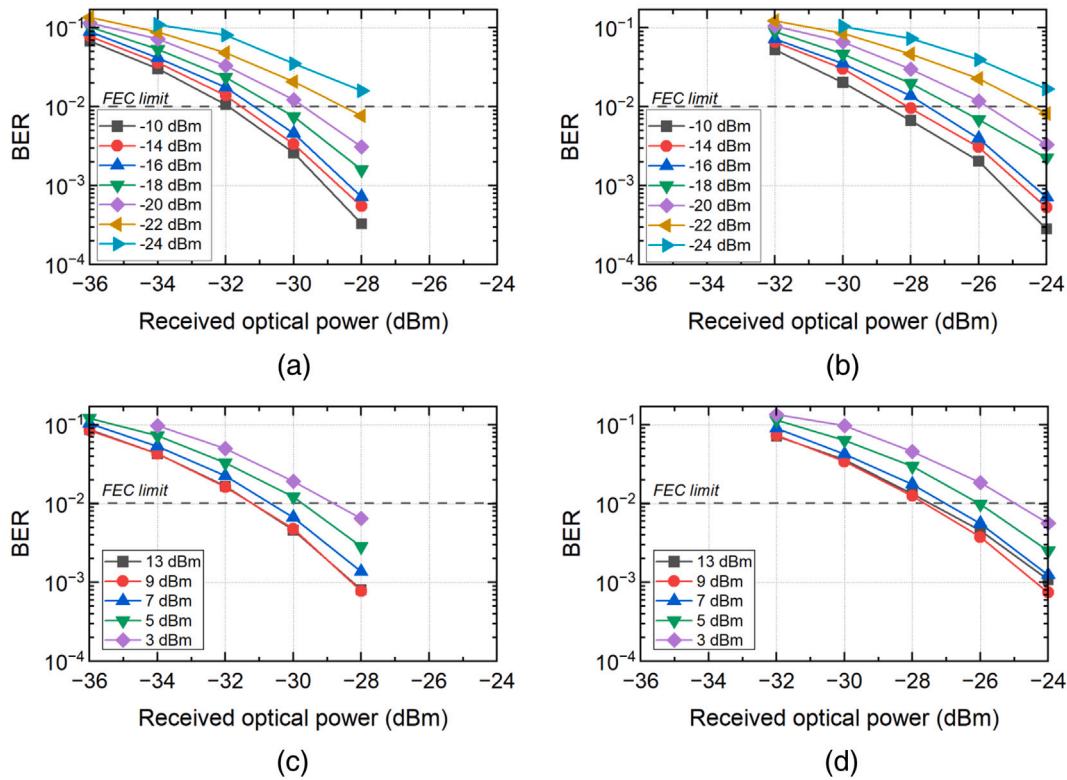


Fig. 6. BER performance of the PTBC-16QAM signals under back-to-back conditions: BER curves for the (a) 120-Gb/s and (b) 240-Gb/s signals as a function of the EDFA input LO power, with the output power fixed at 10.4 dBm; and for the (c) 120-Gb/s and (d) 240-Gb/s signals as a function of the EDFA output LO power, with the input power fixed at -15 dBm.

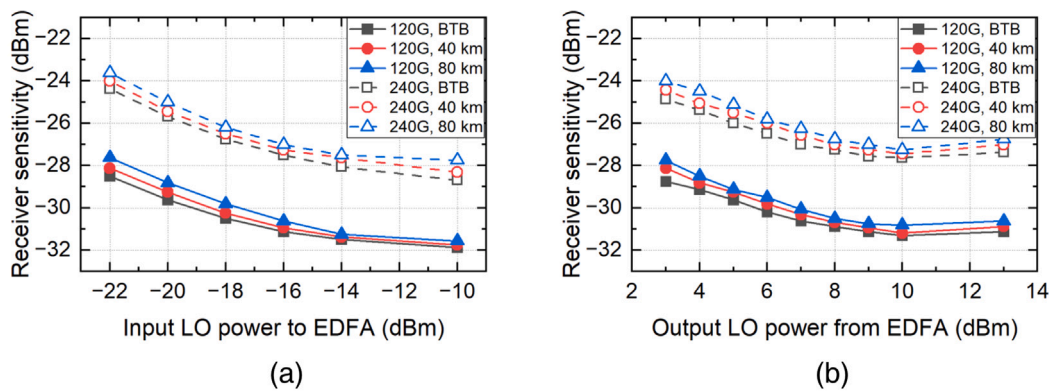


Fig. 7. (a) Receiver sensitivities (at a BER of 10^{-2}) for 120- and 240-Gb/s PTBC-16QAM signals as a function of the EDFA input LO power under various transmission distances. (b) Receiver sensitivities for the same signals as a function of the EDFA output LO power under various transmission distances.

EDFA output LO power dropped below 9 dBm, a gradual degradation in BER performance was observed. A similar trend was also found for the 240-Gb/s signal, as shown in Fig. 6(d).

Fig. 7(a) illustrates the receiver sensitivities (at a BER of 10^{-2}) of the 120- and 240-Gb/s PTBC-16QAM signals as a function of the input LO power to the EDFA. The EDFA output power was fixed at 10.4 dBm. The tap lengths of the PTBC decoder for the 120-Gb/s signals under the back-to-back, 40-km, and 80-km transmission conditions were 11, 17, and 23, respectively, while those for the 240-Gb/s signals were 19, 25, and 31. Both data rates exhibited similar trends: when the input LO power was greater than -14 dBm, the sensitivity penalty was marginal under the back-to-back conditions. However, as the input LO power

decreased below this threshold (corresponding to an LO OSNR below 39 dB), the receiver sensitivity degraded at a rate of approximately 0.5 dB/dB. For both the 120- and 240-Gb/s signals, 80-km transmission resulted in an additional receiver sensitivity penalty of approximately 0.3–0.9 dB, which was consistently observed compared to the back-to-back condition. Fig. 7(b) illustrates the receiver sensitivities of the 120- and 240-Gb/s signals as a function of the output LO power from the EDFA. The EDFA input power was set to -15 dBm, and the back-to-back results were extracted from Figs. 6(c) and 6(d). When the output LO power exceeded 10 dBm, the receiver sensitivities remained nearly constant. However, when the output power dropped below this level, the receiver sensitivity degraded linearly with the output LO power

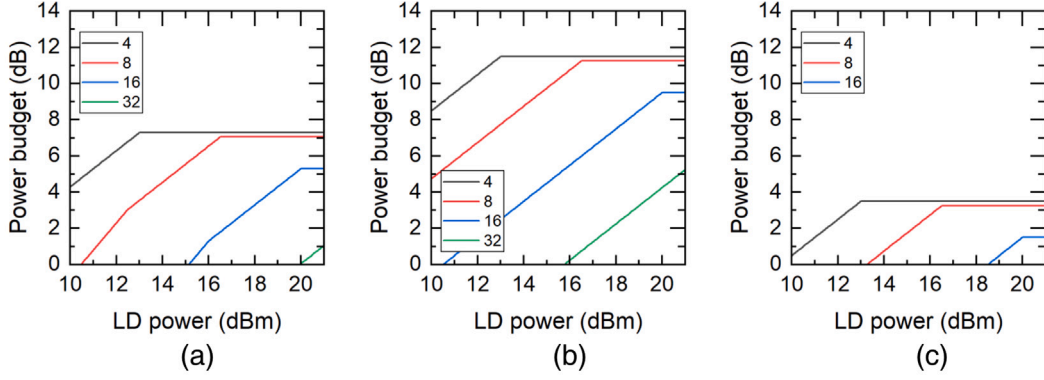


Fig. 8. Estimated power budget as a function of laser output power for the transmission of (a) a 120-Gb/s signal over 80-km SSMF, (b) a 240-Gb/s signal over 40-km SSMF, and (c) a 240-Gb/s signal over 80-km SSMF.

at a rate of approximately 0.5 dB/dB primarily due to the reduced shot-noise dominance [23].

4. Analysis of the number of signal lanes per LO lane

To achieve high transmission efficiency, it is desirable to increase the number of signal lanes that can be detected using a single LO lane. This can be evaluated by analyzing the power budget, which is expressed as

$$P_{\text{budget}} = \begin{cases} P_{\text{SBS,th}} - L_{\text{mod}} - L_{\text{fiber}} - \text{RS} & , P_{\text{LD}} \geq P_{\text{SBS,th}} + 3.5 \log_2 N \\ P_{\text{LD}} - 3.5 \log_2 N - L_{\text{mod}} - L_{\text{fiber}} - \text{RS} & , P_{\text{LD}} < P_{\text{SBS,th}} + 3.5 \log_2 N \end{cases} \quad (6a)$$

$$\text{RS} = \text{RS}_{\text{sat}} - 0.5 \min[P_{\text{LO,OAout}} - P_{\text{LO,OAin,sat}}, 0] - 0.5 \min[P_{\text{LO,OAin}} - P_{\text{LO,OAin,sat}}, 0], \quad (6b)$$

where $P_{\text{SBS,th}}$ is the SBS threshold power, P_{LD} is the output power of the LD, and N is the total number of split lanes at the transmitter, including all signal lanes and one LO lane. L_{mod} denotes the total loss of the DP-IQM, including both insertion and modulation losses, and L_{fiber} is the transmission loss. All power terms in Eq. (6) are expressed on a decibel scale. RS represents the effective receiver sensitivity. As shown in Figs. 4(d) and 4(e), the received LO power did not increase further when the transmitted LO power exceeded 6 dBm due to SBS. We also maintained the signal power below 6 dBm to mitigate fiber nonlinearities, such as self-phase modulation. The power per lane at the transmitter output is calculated as $(P_{\text{LD}} - 3.5 \log_2 N)$, assuming the LO launch power is limited below $P_{\text{SBS,th}}$. The splitting loss was set to 3.5 dB per split to account for practical implementation losses. For simplicity, it is assumed that the signal and LO are split with equal optical power at the transmitter. In addition, as shown in Figs. 7(a) and 7(b), increasing either the LO power launched into the receiver-side OA or the amplified LO power at its output does not further improve the receiver sensitivity beyond a certain point. The corresponding saturation powers at the input and output of the OA are denoted as $P_{\text{LO,OAin,sat}}$ and $P_{\text{LO,OAout,sat}}$, respectively, and the corresponding receiver sensitivity at saturation is denoted as RS_{sat} . The receiver sensitivity penalty was empirically derived from the experimental results in Figs. 7(a) and 7(b), as expressed in Eq. (6b).

We evaluated the power budget using the parameters summarized in Table 1. The insertion loss of the DP-IQM was set to 9 dB, based on the typical loss of commercially available single-polarization IQMs (5–7 dB) and an additional connection loss of 2 dB from two PBSs. The modulation loss was set to 5 dB, assuming that two SRRC-filtered electrical four-level signals with amplitudes of $1.2V_{\pi}$ were applied to the DP-IQM. By varying the roll-off factor of the SRRC filter from 0.1 to 1, the

Table 1

Parameters used for power budget analysis.

Parameter	Value
$P_{\text{SBS,th}}$	6 dBm
Insertion loss of DP-IQM	9 dB
16QAM modulation loss	5 dB
Fiber loss parameter	0.2 dB/km
$P_{\text{LO,OAin,sat}}$	-14 dBm
$P_{\text{LO,OAout,sat}}$	10 dBm
RS_{sat} for 120-Gb/s 16QAM	-31.3 dBm
RS_{sat} for 240-Gb/s 16QAM	-27.5 dBm

resulting modulation loss was calculated to range from 3.3 to 4.8 dB. All other parameters were extracted from our experimental results. Fig. 8(a) shows the calculated power budget for the transmission of 120-Gb/s PTBC-16QAM signals over 80 km of SSMF. The case of $N = 8$ was examined in more detail. When the LD power was below 16.5 dBm (i.e., the LO launch power was lower than the SBS threshold), the power budget decreased in the same proportion as the LD power. However, when the LD power dropped below 12.5 dBm (i.e., the received LO power of $P_{\text{LO,OAin}}$ was lower than $P_{\text{LO,OAin,sat}} = -14$ dBm), the budget degraded more steeply, decreasing by 1.5 dB for every 1 dB drop in LD power. This increased degradation was attributed to the decrease in receiver sensitivity. Based on this analysis, 15 and 31 signal lanes could be supported by a single LO lane when the LD powers were ≥ 15.2 dBm and ≥ 20 dBm, respectively. Figures Figs. 8(b) and 8(c) show the calculated power budget for the transmission of 240-Gb/s PTBC-16QAM signals over 40- and 80-km SSMF, respectively. For the 40-km case, LD powers of at least 10.5 dBm and 15.8 dBm were required to support 15 and 31 signal lanes, respectively. For the 80-km case, LD powers of at least 13.3 dBm and 18.5 dBm were required to support 7 and 15 signal lanes, respectively.

5. Summary

We proposed a shared LO-based coherent-lite architecture for > 100-Gb/s metro networks with an 80-km reach. In this scheme, a single remote LO is transmitted and subsequently amplified at the receiver to serve multiple signal channels, increasing fiber utilization efficiency from $1/2$ to $(N-1)/N$, where N is the total number of split branches. This receiver-side amplification strategy effectively circumvents SBS limitations associated with high-power transmission. Additionally, we utilized the Alamouti PTBC scheme to enable the use of a single-polarization receiver. This combination of PTBC and the self-coherent scheme allows for the removal of CPE taps in the decoder.

We experimentally validated the feasibility of the proposed system by transmitting 120- and 240-Gb/s PTBC-16QAM signals over up to 80 km of SSMF. In the experiment, the launch power of the LO was

kept below 6 dBm to mitigate SBS. The receiver sensitivity (at a BER = 10^{-2}) degraded at a rate of 0.5 dB/dB when the received LO power at the EDFA input fell below -14 dBm, primarily due to the reduced LO OSNR. Similarly, a degradation rate of 0.5 dB/dB was observed when the amplified LO power at the output dropped below 9 dBm, which was attributed to the reduced shot-noise dominance. We presented a comprehensive power budget analysis based on this sensitivity degradation rate. According to this analysis, assuming a realistic modulator loss of 9 dB and a 16-dBm LD output power, a single LO can support up to 15 (for 120 Gb/s) and 7 (for 240 Gb/s) signal lanes for 80-km transmission, corresponding to fiber utilization efficiencies of 93.8% and 87.5%, respectively.

CRedit authorship contribution statement

Jongwan Kim: Writing – review & editing, Validation, Methodology, Investigation, Formal analysis, Data curation, Conceptualization. **Sang-Rok Moon:** Writing – review & editing, Methodology, Formal analysis, Conceptualization. **Sun Hyok Chang:** Writing – review & editing, Methodology, Formal analysis, Conceptualization. **Hun-Sik Kang:** Project administration, Funding acquisition, Conceptualization. **Sunghyun Bae:** Writing – review & editing, Writing – original draft, Validation, Methodology, Investigation, Formal analysis, Data curation, Conceptualization.

Funding

This work was supported by Institute for Information and Communications Technology Promotion (IITP) grant funded by the Ministry of Science and ICT, South Korea (2021-0-00809, Development of Tbps Optical Communication Technology).

Declaration of competing interest

The authors declare the following financial interests/personal relationships which may be considered as potential competing interests: Jongwan Kim reports financial support was provided by Institute for Information and Communications Technology Promotion. Sang-Rok Moon reports financial support was provided by Institute for Information and Communications Technology Promotion. Sun Hyok Chang reports financial support was provided by Institute for Information and Communications Technology Promotion. Hun-Sik Kang reports financial support was provided by Institute for Information and Communications Technology Promotion. Sunghyun Bae reports financial support was provided by Institute for Information and Communications Technology Promotion. If there are other authors, they declare that they have no known competing financial interests or personal relationships that could have appeared to influence the work reported in this paper.

Data availability

Data will be made available on request.

References

- [1] C. Xie, B. Zhang, Scaling optical interconnects for hyperscale data center networks, *Proc. IEEE* 110 (11) (2022) 1699–1713.
- [2] K. Wang, J. Zhang, Y. Wei, L. Zhao, W. Zhou, M. Zhao, J. Xiao, X. Pan, B. Liu, X. Xin, et al., 100-Gbit/s/ λ PAM-4 signal transmission over 80-km SSMF based on an 18-GHz EML at O-band, in: *Optical Fiber Communication Conference*, Optica Publishing Group, 2020, pp. Th1D–5.
- [3] H. Wakita, M. Nagatani, Y. Ogiso, M. Nakamura, F. Hamaoka, Y. Shiratori, T. Kobayashi, Y. Miyamoto, H. Takahashi, 100-GHz-bandwidth InP-based on-board coherent Tx front-end enabling 2-Tb/s/ λ optical transmission, in: *Optical Fiber Communication Conference*, Optica Publishing Group, 2024, pp. Th4C–2.
- [4] W. Li, C. St-Arnault, Z. Wei, M.S. Alam, S. Yamauchi, H. Asakura, B. Beggs, N. Ben-Hamida, D.V. Plant, Net 200 Gbps O-band IM/DD transmission over 80 km SMF using InP EML with sub 1-Vpp driving signal and QD-SOA, in: *ECOC 2024; 50th European Conference on Optical Communication*, VDE, 2024, pp. 55–58.
- [5] W. Li, M. Zhang, Y. Zeng, Y. Chen, J. Chen, Y. Li, M. Tang, SOA enabled self-homodyne coherent bidirectional transmission for metro-datacenter interconnects, *J. Lightwave Technol.* 41 (9) (2023) 2601–2612.
- [6] Y. Zhu, L. Yi, B. Yang, X. Huang, J.S. Wey, Z. Ma, W. Hu, Comparative study of cost-effective coherent and direct detection schemes for 100 Gb/s/ λ PON, *J. Opt. Commun. Netw.* 12 (9) (2020) D36–D47.
- [7] G. Rizzelli, M. Casasco, V. Ferrero, A. Pagano, R. Gaudino, Analysis and experimental demonstration of possible architectures for future coherent metro+PON converged networks, *J. Opt. Commun. Netw.* 17 (2) (2025) A142–A154.
- [8] M.S. Faruk, H. Louchet, M.S. Erkilinç, S.J. Savory, DSP algorithms for recovering single-carrier Alamouti coded signals for PON applications, *Opt. Express* 24 (21) (2016) 24083–24091.
- [9] X. Chen, S. Chandrasekhar, P. Winzer, Self-coherent systems for short reach transmission, in: *2018 European Conference on Optical Communication*, ECOC, 2018, pp. 1–3.
- [10] W. Wang, D. Zou, Z. Wu, Q. Sui, D. Huang, C. Lu, F. Li, Alamouti coding enabled polarization insensitive simplified self-homodyne coherent system for short-reach optical interconnects, *Opt. Laser Technol.* 182 (2025) 112164.
- [11] M. Erkilinç, R. Emmerich, K. Habel, V. Jungnickel, C. Schmidt-Langhorst, C. Schubert, R. Freund, PON transceiver technologies for ≥ 50 Gbits/s per λ : Alamouti coding and heterodyne detection, *J. Opt. Commun. Netw.* 12 (2) (2020) A162–A170.
- [12] S.-R. Moon, S. Bae, Coherent-lite PON with repetition code and single polarization receiver, *Opt. Commun.* (ISSN: 0030-4018) 557 (2024) 130331.
- [13] P.M. Krummrich, K. Kotten, Extremely fast (microsecond timescale) polarization changes in high speed long haul WDM transmission systems, in: *Optical Fiber Communication Conference*, Optica Publishing Group, 2004, p. FI3.
- [14] W. Wang, Z. Zhou, Y. Zeng, J. Liu, G. Yao, H. Wu, Y. Ding, S. Zhou, S. Yan, M. Tang, CMOS-compatible high-speed endless automatic polarization controller, *APL Photonics* 9 (6) (2024).
- [15] A. Hraghi, G. Rizzelli, A. Pagano, V. Ferrero, R. Gaudino, Analysis and experiments on C band 200G coherent PON based on Alamouti polarization-insensitive receivers, *Opt. Express* 30 (26) (2022) 46782–46797.
- [16] P. Torres-Ferrera, M.S. Faruk, I.B. Kovacs, S.J. Savory, Parallel adaptive equalizer for Alamouti-coded signals recovery in simplified coherent PON, *IEEE Photonics Technol. Lett.* 36 (10) (2024) 633–636.
- [17] H.Y. Rha, S.-R. Moon, S.-H. Chang, J.-Y. Oh, H.-S. Kang, Feedforward phase estimation for real-time PTBC decoding in high-speed optical access networks, *J. Lightwave Technol.* 42 (13) (2024) 4394–4401.
- [18] R. Zhang, K. Kuzmin, Y.-W. Chen, W.I. Way, 800G/ λ self-homodyne coherent links with simplified DSP for next-generation intra-data centers, *J. Lightwave Technol.* 41 (4) (2023) 1216–1222.
- [19] T. Sasaki, F. Sato, B.G. Risch, P.A. Weimann, Ultrahigh fiber count and high-density cables, deployments, and systems, *Proc. IEEE* 110 (11) (2022) 1760–1771.
- [20] B. Zhu, T.F. Taunay, M.F. Yan, J.M. Fini, M. Fishteyn, E.M. Monberg, F.V. Dimarcello, Seven-core multicore fiber transmissions for passive optical network, *Opt. Express* 18 (11) (2010) 11117–11122.
- [21] S.-R. Moon, J. Kim, S.H. Chang, H.-S. Kang, S. Bae, 120-Gb/s PTBC-aided self-coherent PON system, in: *2024 Opto-Electronics and Communications Conference*, OECC, 2024, pp. 1–3.
- [22] S.J. Savory, Digital filters for coherent optical receivers, *Opt. Express* 16 (2) (2008) 804–817.
- [23] K. Kikuchi, Fundamentals of coherent optical fiber communications, *J. Lightwave Technol.* 34 (1) (2015) 157–179.